

New analytical solution for the calculation of the acoustic diffraction field around a rigid edge in time and frequency domain

Petros Nikolaou¹, Anastasia Marketou², Sotirios Salagas¹, Penelope Menounou¹
¹Department of Mechanical Engineering and Aeronautics, University of Patras,
University of Patras Campus, 26504, Patras, Greece.
²Department of Flow Physics and Technology, Aerospace Engineering, TU Delft,
Mekelweg 5, 2628 CD Delft, Netherlands.

ABSTRACT

Analytical approximate solutions for the diffraction by a rigid wedge are derived in both frequency and time domain. The analysis starts with the exact solution in time domain. A new type of plot is presented which helps to understand how diffraction evolves around the boundaries of geometrical acoustics discontinuity. Analytical approximate solution for all types of incident radiation are presented as short time asymptotics of the exact solutions in time domain. The three solutions are presented in a unified form. Finally, using the Fourier transform approximate solutions are obtained in the frequency domain in a unified form for all types of incident radiation.

Νέα αναλυτική λύση για τον υπολογισμό του ακουστικού πεδίου περίθλασης γύρω από ακουστικά σκληρή σφήνα στο πεδίο του χρόνου και στο πεδίο των συχνοτήτων

ΠΕΡΙΛΗΨΗ

Αναλυτικές προσεγγιστικές λύσεις για την περίθλαση από μία ακουστικά σκληρή σφήνα προτείνονται τόσο στο πεδίο των συχνοτήτων όσο και στο πεδίο του χρόνου. Η ανάλυση ξεκινά με την ακριβή λύση στο πεδίο του χρόνου. Παρουσιάζεται ένας νέος τύπος γραφήματος που βοηθά στην κατανόηση του τρόπου με τον οποίο η περίθλαση εξελίσσεται γύρω σύνορα της ασυνέχειας του γεωμετρικού ακουστικού πεδίου. Αναλυτικές προσεγγιστικές λύσεις για όλους τους τύπους της προσπίπτουσας ακτινοβολίας παρουσιάζονται ως ασυμπτωτικές μικρών χρόνων των ακριβών λύσεων στο πεδίο του χρόνου. Οι τρεις λύσεις παρουσιάζονται σε μια ενιαία μορφή. Τέλος, χρησιμοποιώντας το μετασχηματισμό Fourier, προσεγγιστικές λύσεις λαμβάνονται στο πεδίο των συχνοτήτων σε μια ενιαία μορφή για όλους τους τύπους προσπίπτουσας ακτινοβολίας.

Introduction

Mathematical solutions for the diffraction field around a wedge appeared more than a century ago. The reader is referred to the work of ref. [1] for a review of rigorous solutions. Many analytical approximate solutions appeared over time as asymptotics of rigorous formulas in both time and frequency domain. Detail presentation of the analytical approximate solutions can be found in the introduction sections of ref [2] (for time domain) and ref [3] (for frequency domain). The benefit of the approximate solutions is that they are easier to calculate compared to the rigorous solutions and they also can provide benefits in physical interpretation of the diffraction phenomenon.

In this paper new analytical approximate solutions for the diffraction of a spherical wave by a rigid wedge are presented in both time and frequency domain. The study starts with a review of the exact solution in time domain. A new type of diffraction field plot is introduced, which aims to contribute to the understanding of diffraction formulation. A solution is initially derived as short time asymptotic of the exact solution in time domain. An approximate solution in frequency domain is then obtained using the Fourier transform. Finally, approximate solutions for cylindrical and plane waves are presented and the solution is reformulated into a unified form for all types of incident radiation.

1. Exact Solution in time domain

The studied solution was derived in a previous work of the authors' [2] as an approximation of the Biot-Tolstoy exact solution valid for short times. In the following we present the formulations of the Biot-Tolstoy the authors' approximate formula in the form of impulse responses.

The Biot-Tolstoy formula is given by:

$$P_{exact} = \sum_{j=1}^4 P_{exact}^j = \sum_{j=1}^4 -\frac{c}{2\gamma\pi} \frac{1}{r_S r_R} \frac{1}{\sinh(\zeta)} \frac{\sin(b_j)}{\cosh\left(\frac{\zeta}{\gamma}\right) - \cos(b_j)},$$

$$\zeta = \cosh^{-1}(F), \quad F = \frac{c^2 t^2 - r_S^2 - r_R^2 - (z_R - z_S)^2}{2rr_0} \quad (1.1)$$

$$b_j = \pm \frac{\theta_R}{\gamma} \pm \frac{\theta_S}{\gamma} + \frac{\pi}{\gamma}, \quad \gamma\pi = 2\pi - 2\Omega$$

where c is the speed of sound (θ_S, r_S, z_S) and (θ_R, r_R, z_R) are the source and receiver coordinates on a cylindrical frame of reference that has the edge of the wedge (z -axis) as symmetry axis z . The diffraction signal arrives to the receiver at time $t=L/c$, where L is the least diffraction path $L = \sqrt{(r_S + r_R)^2 + (z_S - z_R)^2}$. A detailed presentation of the wedge geometry is shown in Fig. 1 of ref [2]. The terms F and ζ are functions of time t and distances r_S, z_S, r_R, z_R , while the terms b_j are functions of the source, receiver and wedge angles $\theta_R, \theta_S, \Omega$. The solution is

summation of 4 similar terms that only have different terms b_j . In the present paper, b_j terms are defined as

$$\begin{aligned} b_1 &= -\frac{\theta_R}{\gamma} + \frac{\theta_S}{\gamma} + \frac{\pi}{\gamma}, b_2 = \frac{\theta_R}{\gamma} + \frac{\theta_S}{\gamma} + \frac{\pi}{\gamma}, \\ b_3 &= -\frac{\theta_R}{\gamma} - \frac{\theta_S}{\gamma} + \frac{\pi}{\gamma}, b_4 = \frac{\theta_R}{\gamma} - \frac{\theta_S}{\gamma} + \frac{\pi}{\gamma} \end{aligned} \quad (1.2)$$

. As it will be shown in the following b_j are important parameters for the diffraction problem and henceforth they will be called *diffraction angles*.

The unit step response of the Biot -Tolstoy can be calculated as,

$$P_{exact}^{us} = \sum_{j=1}^4 P_{exact}^{us,j} = \sum_{j=1}^4 \int_{L/c}^t P_{exact}^j dt, \quad (1.3)$$

Despite the singularity of the impulse response, it can be proven that the unit step response is not singular. Specifically, one can express P_{exact}^j as,

$$\begin{aligned} P_{exact}^j &= \frac{-sign(\sin b_j)}{c\pi t} \frac{\partial M_j}{\partial t}, \\ M_j &= \arctan \left[\frac{\tanh\left(\frac{1}{2\gamma} \operatorname{arccos} h(F)\right)}{d_j} \right], d_j = \sqrt{\frac{1 - \cos b_j}{1 + \cos b_j}} \end{aligned} \quad (1.4)$$

then the Hölder inequality yields:

$$\left| P_{exact}^{us,j} \right| = \left| \int_{L/c}^t P_{exact}^j dt \right| \leq \int_{L/c}^t \left| P_{exact}^j \right| dt \leq \left\| \frac{1}{c\pi t} \right\|_{\infty} \cdot \left\| \frac{\partial M_j}{\partial t} \right\|_1 = \frac{|M_j|}{\pi L} \quad (1.5),$$

where $\left\| \frac{1}{c\pi t} \right\|_{\infty} = \operatorname{ess\,sup} \left(\frac{1}{c\pi t} \right) = \max \left(\frac{1}{c\pi t} \right) = \frac{1}{c\pi L/c} = \frac{1}{\pi L}$ ('ess sup' is the essential supremum) and $\left\| \frac{\partial M_j}{\partial t} \right\|_1 = \int_{L/c}^t \left| \frac{\partial M_j}{\partial t} \right| dt = |M_j|$ the first norm of $\left| \frac{\partial M_j}{\partial t} \right|$.

Thus, it is proven that $P_{exact}^{us,j}$ is bounded.

2. Diffraction Signal new type of plots

The exact unit step response can be found by Eq. (1.3) with no singularities using a numerical quadrature technique. The authors have used the 'quadgk' command of MATLAB which is based on adaptive Gauss-Kronrod quadrature.

The diffraction signal depends primarily on the angle parameters $\theta_R, \theta_S, \Omega$. The shadow boundaries divide the diffraction field in regions that contain different number of geometrical acoustics contributions (incidence or reflections). For an open wedge the two shadow boundaries are the shadow boundary of incidence and the shadow boundary of reflection from the face of the wedge facing the source or the shadow boundaries of the reflections from both wedge faces. For closed wedges

the signal might be subject to multiple reflections before reaching the receiver. Starting from one face of the edge multiple reflections occur between the faces. The phenomenon stops when the last reflection does not illuminate the opposing edge, thus creating a shadow boundary. The same process is repeated starting from the other face of the wedge to determine the other shadow boundary. This last reflection is called *exiting reflection*. For closed wedges, the shadow boundary is the plane determined by the image source of the exiting reflection (named *exiting image source*) and the edge line. For open it is the plane determined by the image source of the sources of reflection or the actual source and the edge line. The magnitude of the exiting reflections, or first reflections, or incident signal is represented by $1/R_l$, where R_l is the distance of the receiver and the corresponding image source or source. The angular locations of the shadow boundaries $\theta_{b_1}, \theta_{b_2}$ and of the image source $\theta_{is_1}, \theta_{is_2}$ differ by π . The shadow boundary angular locations can be found by:

$$\begin{aligned} \frac{\theta_{b_1}}{\gamma} &= s_1 \frac{\pi + \theta_s}{\gamma}, \quad s_1 = \text{sign} \left[\sin \left(\frac{\pi + \theta_s}{\gamma} \right) \right] \\ \frac{\theta_{b_2}}{\gamma} &= s_2 \frac{\pi - \theta_s}{\gamma}, \quad s_2 = \text{sign} \left[\sin \left(\frac{\pi - \theta_s}{\gamma} \right) \right] \end{aligned} \quad (2.1)$$

and thus,

$$\begin{aligned} \theta_{is_1} &= \theta_{b_1} + \pi \\ \theta_{is_2} &= \theta_{b_2} + \pi \end{aligned} \quad (2.2)$$

Based on the sign parameters s_1, s_2 Eq. (1.2) can be reformulated as,

$$\begin{aligned} b_1 &= -\frac{\theta_R}{\gamma} + s_1 \frac{\theta_{b_1}}{\gamma}, \quad b_2 = \frac{\theta_R}{\gamma} + s_1 \frac{\theta_{b_1}}{\gamma}, \\ b_3 &= -\frac{\theta_R}{\gamma} + s_2 \frac{\theta_{b_2}}{\gamma}, \quad b_4 = \frac{\theta_R}{\gamma} + s_2 \frac{\theta_{b_2}}{\gamma} \end{aligned} \quad (2.3)$$

Equation (2.3) allows us to interpret the terms b_j as normalized distances between θ_R or $-\theta_R$ from the shadow boundary locations θ_{b_1} and θ_{b_2} . Specifically, it can be proven that:

$$\begin{aligned} \text{for } s_1 = '+' , & \begin{cases} \left| p_{exact}^{us,1} \right| = \left| p_{exact}^{us,1} \right|_{\max} = \frac{1}{2R_1} & \text{at } b_1 = 0 \Leftrightarrow \theta_R = \theta_{b_1} \\ \left| p_{exact}^{us,2} \right| = \left| p_{exact}^{us,2} \right|_{\max} & \text{at } |b_2|_{\min}, b_2 \neq 0 \end{cases} \\ \text{for } s_1 = '-' , & \begin{cases} \left| p_{exact}^{us,1} \right| = \left| p_{exact}^{us,1} \right|_{\max} & \text{at } |b_1|_{\min}, b_1 \neq 0 \\ \left| p_{exact}^{us,2} \right| = \left| p_{exact}^{us,2} \right|_{\max} = \frac{1}{2R_1} & \text{at } b_2 = 0 \Leftrightarrow \theta_R = \theta_{b_1} \end{cases} \end{aligned} \quad (2.4)$$

Same holds for s_2 and the parameters b_3, b_4 . From the two factors $p_{exact}^{us,1}$ and $p_{exact}^{us,2}$ associated with the shadow boundary BI only one handles the discontinuity of the geometrical acoustic signal at the shadow boundary. For example, for $s_1 = '+'$ only

b_1 becomes zero in $0 \leq \theta_R \leq \gamma\pi$ and thus only $|p_{exact}^{us,1}|$ becomes half of the geometrical acoustic field $1/R_1$, $|p_{exact}^{us,1}|$ then decreases until it reaches a minimum at $\theta_R = \theta_{b_1} + \pi$. Consider now a Riemann space defined as $-\gamma\pi \leq \theta_R \leq 0$. Then consider Eq. (1.3) in the union of physical and Riemann spaces $-\gamma\pi \leq \theta_R \leq \gamma\pi$. For $s_1 = '+'$, it is $b_2 = 0$ and it is $|p_{exact}^{us,2}|$ that becomes half of the geometrical acoustic field $1/R_1$ at $\theta_R = -\theta_{b_1}$. $|p_{exact}^{us,2}|$ then decreases until it reaches a minimum at $\theta_R = -\theta_{b_1} + \pi$. The locations $\theta_R = -\theta_{b_1}$ and $\theta_R = -\theta_{b_2}$ are considered angular locations of shadow boundaries of an imaginary source-wedge-receiver in Riemann space. In short, these shadow boundaries are called *Riemann Boundaries*. In conclusion, we can define the diffraction angles b_j as normalized distances of the receiver from the shadow boundaries or the Riemann boundaries.

The diffraction angles are significant parameters of the diffraction study. In the present paper we propose a way to visualize the diffraction signal as it changes with the angles $\theta_R, \theta_S, \Omega$. A figure of $p_{exact}^{us,j}$ contours vs b_j and Ω can be created representing all terms b_j ($j=1,2,3,4$) and $p_{exact}^{us,j}$. This figure is named *diffraction map* because for a given set of $\theta_R, \theta_S, \Omega$ each value of $p_{exact}^{us,1}, p_{exact}^{us,2}, p_{exact}^{us,3}, p_{exact}^{us,4}$, can be found on the graph at the locations $(b_1, \Omega), (b_2, \Omega), (b_3, \Omega), (b_4, \Omega)$, respectively [see Figure 2.1(a)]. Furthermore, each pair of angles (b_j, Ω) can be visualized in a polar plot see Figure 2.1(b). Each polar plot resembles a clock with two hands, one indicating the wedge half angle, *the wedge angle hand*, and another indicating the angle b_j , *the diffraction angle hand*.

The diffraction signal becomes maximum at $b_j = 0$, which corresponds to the location of a shadow boundary and minimum at the location of the corresponding image source $b_j = \pi$ or $-\pi$.

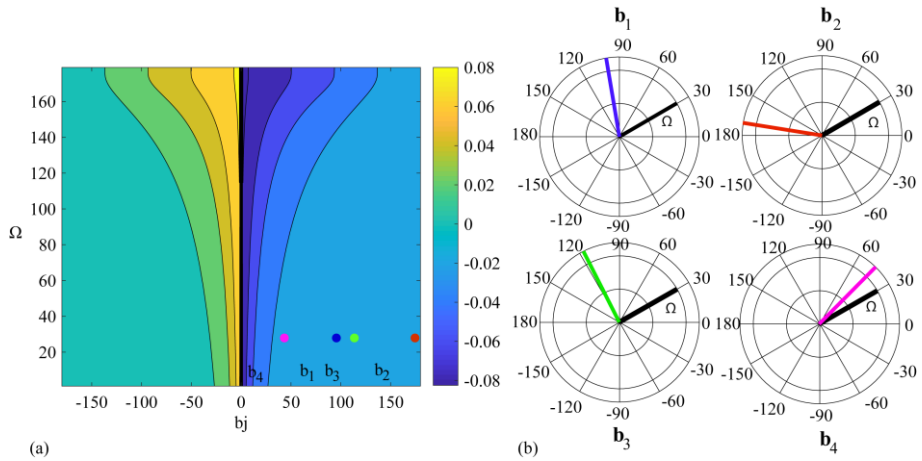


Figure 2.1 a) contours of p_{exact}^j versus (b_j, Ω) ; b) an example of (b_j, Ω) for the 4 terms of p_{exact}^j .

3. Analytical approximate time domain solution

The authors' approximate impulse response comes derives from the Biot-Tolstoy for short times. Specifically, for $\zeta \ll 1$, $\zeta/\gamma \ll 1$ the Biot-Tolstoy formula is approximated by,

$$p_{ijf} = \sum_{j=1}^4 p_{ijf}^j = \sum_{j=1}^4 -\frac{1}{4\gamma\pi} \sqrt{\frac{2c}{r_R r_S L}} \frac{1}{\sqrt{\tau}} \frac{h \sin(b_j)}{\tau + h[1 - \cos(b_j)]}, \quad (3.1)$$

where L is the length of the least diffraction path, h a distance parameter with, $h = \gamma^2 r_R r_S / cL$, and τ the time that starts counting the time when diffraction is first pereceived by the receiver (L/c). It is $\tau = t - L/c$. τ is called diffraction time.

As opposed to the Biot-Tolstoy the unit step response for our proposed solution can be found analytically. The proposed approximate unit step response is:

$$P_{appr}^{us} = \sum_{j=1}^4 P_{appr}^{us,j} = \sum_{j=1}^4 -\frac{1}{4\gamma\pi} \sqrt{\frac{2c}{r_R r_S L}} h \sin(b_j) \frac{2}{\sqrt{\tau_{lag}^j}} \arctan\left(\sqrt{\frac{\tau}{\tau_{lag}^j}}\right), \quad (3.2)$$

where $\tau_{lag}^j = h[1 - \cos(b_j)]$ a time parameter. Similar to b_j , τ_{lag}^j expresses the proximity of the receiver to the shadow boundary as described by Eq. (2.4). τ_{lag}^j , however also expresses the proximity of the receiver and the source to the edge and also becomes smaller as the wedge angle decreases.

Figure 3.1 shows contours of the exact unit step calculation and of Eq. (1.3) at several diffraction times τ . Good agreement between the two solutions is observed for the two shorter times, while differences between the two solutions appear for two larger times. Numerical experimentation has shown that the proposed approximate solution yields less than 5% error ($error = 100 |p_{appr}^{us} - p_{exact}^{us}| / |p_{exact}^{us}|$) for $\tau \leq 0.02 \cdot \pi r_S r_R / L \cdot c$ and $\Omega \leq 160$.

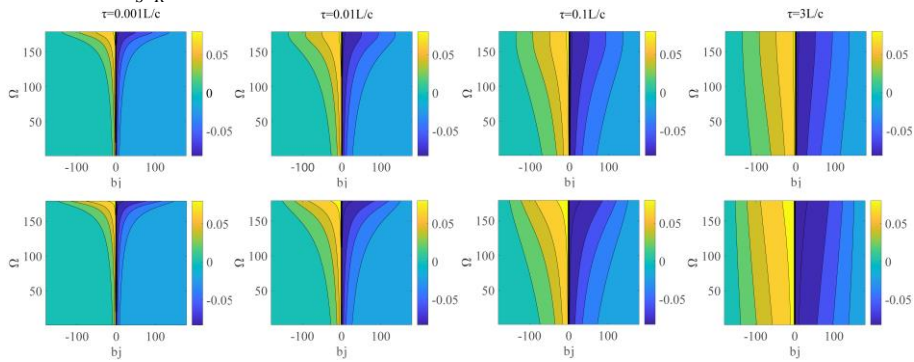


Figure 3.1. (first row) contours of $p_{exact}^{us,j}$ versus (b_j, Ω) ; (second row) contours of $p_{appr}^{us,j}$ versus (b_j, Ω) for several times.

As opposed to another approximate solution derived previously by the authors, the approximate solution presented in this paper has an extended region of validity. Furthermore, the proposed solution has the same time dependence namely $(1/\sqrt{\tau})[1/(\tau + \tau_{lag}^j)]$ as the previously derived solution. As a result, the proposed solution retains the benefits of the solution in ref.. Those are: i) The impulse response is integrable and the primitive functions of the impulse response can be found analytically. The primitive functions can be used to compute analytically the convolution integral that describe the diffraction response caused by an arbitrary signal (see ref). Furthermore, the second primitive function can be used to accelerate the numerical calculation of the convolution integral by orders of magnitude. (see also ref.). ii) It can be proven that the impulse response of a source-wedge-receiver configuration is equal to the impulse response of another source-edge-receiver configuration on a half-plane. In other words, all source-wedge-receiver problems can be solved simply by solving an equivalent and simpler half-plane problem. This property is named *mapping property*. iii) A normalized time can be defined in which the impulse response or primitive function for all source-wedge-receiver configurations can be represented by a single curve. The normalized time is called *diffraction number* and the curve *generator curve*. iv) The analytical Fourier transform of the impulse response can be found leading to an approximate diffraction solution in frequency domain.

4. Analytical approximate frequency domain solution

The Fourier transform of the impulse response of Eq. (3.1) yields:

$$P_d = \sum_{j=1}^4 P_d^j = \sum_{j=1}^4 -i \frac{1}{L} e^{i(kL - \frac{\pi}{4}) - i\omega\tau_{lag}^j} \frac{\sin(b_j)}{2\sqrt{1 - \cos(b_j)}} \left[\frac{1-i}{2} + iF \left(\sqrt{\frac{2}{\pi}} \omega\tau_{lag}^j \right) \right], \quad (4.1)$$

where ω is the angular frequency of the source. Good agreement has been observed as frequency increases. Specifically, numerical experimentation has shown that relative error for the magnitude of the two solutions remains under 5% for frequencies $f \leq \pi r_s r_R / Lc$ and wedge angle $\Omega \leq 155^\circ$. Also note, that Eq. (4.1) has similar form to another solution presented by the authors in ref. [3]. As a result Eq. (4.1) can also be used to handle diffraction by directional sources (see ref. [3] for details).

5. Unified form for all types of incident signals

Approximate solutions for wedge diffraction in time domain and frequency domain are presented in a unified form for all types of incident radiation. The approximate solutions are derived for plane and cylindrical incidence using the methodology presented in ref. [2] for the spherical incidence.

In time domain the solutions are:

$$P_d = \sum_{j=1}^4 P_d^j = \sum_{j=1}^4 -i P_{amp} P_{spr} * D^j, P_{amp} = \begin{cases} -c / 2\gamma\pi r_R r_S & \text{sph} \\ -c \sqrt{\frac{c}{\gamma\pi^2 r_R}} \frac{H_0^{(1)}(t-r_S/c)}{\sqrt{t^2 - r_S^2/c^2}} & \text{cyl} \\ -c / 2\gamma\pi r_R & \text{pl} \end{cases}$$

$$P_{spr} = \begin{cases} \frac{\sqrt{r_R}}{\sqrt{2c}\sqrt{t}}, \text{ pl} \\ \frac{\sqrt{r_S r_R} H(t-r_R/c) \sqrt{t-r_S/c}}{c\sqrt{(\tau+r_S/c)(r_S/c+2L/c)}}, \text{ cyl} \\ \frac{\sqrt{r_S r_R}}{\sqrt{t}\sqrt{2cL}}, \text{ sph} \end{cases}, D^j = \begin{cases} \frac{\sin(b_j)}{1 + \frac{c}{r_R \gamma^2} - \cos(b_j)}, \text{ pl} \\ \frac{\sin(b_j)}{1 + \frac{c^2 [\tau + r_S/c][r_S/c + 3L/c]}{2r_R r_S \gamma^2} - \cos(b_j)}, \text{ cyl} \\ \frac{\sin(b_j)}{1 + \frac{\tau c L}{\gamma^2 r_S r_R} - \cos(b_j)}, \text{ sph} \end{cases}, (5.1)$$

where (*) denotes convolution only for the case of cylindrical radiation. In the two other cases (*) reduces to simple multiplication. The Fourier transform of Eq.(5.1) yields the following frequency domain approximate solutions:

$$P_d = \sum_{j=1}^4 P_d^j = \sum_{j=1}^4 -i P_{amp} P_{spr} D^j \Psi^j, P_{amp} = \begin{cases} 1/L & = P_{amp,sph} & \text{sph.} \\ H_0^{(1)}(kr_S) & = P_{amp,cyl} & \text{cyl.} \\ 1 & = P_{amp,pl} & \text{pl.} \end{cases}$$

$$P_{spr} = \begin{cases} e^{i(kL - \frac{\pi}{4})} & \text{sph.} \\ \sqrt{\frac{r_S}{L}} e^{i(kr_R - \frac{\pi}{4})} & \text{cyl.}, L = \begin{cases} \sqrt{(r_R + r_S)^2 + (z_R - z_S)^2} & = L_{sph} & \text{sph.} \\ r_R + r_S & = L_{cyl} & \text{cyl.} \\ r & = L_{pl} & \text{pl.} \end{cases} \\ e^{i(kr_R - \frac{\pi}{4})} & \text{pl.} \end{cases} (5.2)$$

$$D^j = \frac{\sin(b_j)}{2\sqrt{1 - \cos(b_j)}}, \Psi^j = e^{-i\omega\tau_{lag}^j} \left[\frac{1-i}{2} + iF \left(\sqrt{\frac{2}{\pi}} \omega\tau_{lag}^j \right) \right]$$

References

- [1] J. J. Bowman, T. B. Senior, and P. L. Uslenghi, Electromagnetic and acoustic scattering by simple shapes (Revised edition), (North-Holland Pub. Co, New York, 1987).
- [2] P. Menounou, M. I. Spiropoulos, and P. Nikolaou, “ Approximate time domain solution for studying infinite wedge diffraction, its parameters, and characteristics,” J. Acoust. Soc. Am. 153 (2), 1399–1411 (2023).
- [3] P. Menounou and P. Nikolaou, “An extension to the directive line source model for diffraction by half planes and wedges,” Acust. Acta united Acust. 102, 307–321 (2016).
- [4] Shampine, L.F. "Vectorized Adaptive Quadrature in MATLAB®." J. Comp. and Appl. Math. Vol. 211, 131–140 (2008).